Title

Advancement of analytical modes in a multichannel, microfluidic droplet-based sample chopper employing phase-locked detection

Journal

Analytical Methods, 10(28)

ISSN

1759-9660

Authors

Negou, Jean T
Hu, Juan
Li, Xiangpeng
et al.

Publication Date

2018-07-28

DOI

10.1039/c8ay00947c

Peer reviewed

HHS Public Access

Author manuscript

Anal Methods. Author manuscript; available in PMC 2019 July 28.

Published in final edited form as:

Anal Methods. 2018 July 28; 10(28): 3436–3443. doi:10.1039/C8AY00947C.

Advancement of analytical modes in a multichannel, microfluidic droplet-based sample chopper employing phase-locked detection

Jean T. Negou[a], **Juan Hu**[a], **Xiangpeng Li**[a,b], and **Christopher J. Easley**[a,*]

[a]Department of Chemistry and Biochemistry, Auburn University, Auburn, AL 36849, USA

Abstract

In this work, we expand upon our recently developed droplet-based sample chopping concepts by introducing a multiplexed fluidic micro-chopper device (μChopper). Six aqueous input channels were integrated with a single oil input, and each of these seven channels was controlled by a pneumatic valve for automated sampling through software control. This improved design, while maintaining high precision in valve-based droplet generation at bandwidths of 0.03 to 0.05 Hz, enabled a variety of analytical modes to be employed on-chip compared to previous devices limited to sample/reference alternations. The device was analytically validated for real-time, continuous calibration with a single sample and five standards; multiplexed analysis during calibration using a mixed mode; and standard addition through spiking of six sample droplets with varying amounts of standard. Finally, the standard addition mode was applied to protein quantification in human serum samples using on-chip, homogeneous fluorescence immunoassays. Ultimately, with only ~1.2 μL of total analyzed solution volume— representing 100-fold and 75-fold reductions in reagent and serum volumes, respectively—we were able to generate full, six-point standard addition curves in only 1.5 min, and results correlated well with those from standard plate-reader equipment. This work thus exploited microfluidic valves for both their automation and droplet phase-locking capabilities, resulting in a micro-analytical tool capable of complex analytical interrogation modes on sub-microliter sample volumes while also leveraging drastic noise rejection via lock-in detection. The multichannel μChopper device should prove particularly useful in analyzing precious biological samples or for dynamic analyses at small volume scales.

Graphical Abstract

Multichannel droplet-based microfluidic sample chopper (μChopper) allows continuous calibration, nanoliter sampling, and protein quantification in human serum.

*Address correspondence to chris.easley@auburn.edu.

[b]Current address: Department of Bioengineering and Therapeutic Sciences, University of California, San Francisco, CA 94158, USA

Electronic Supplementary Information (ESI) available: Additional materials, methods, figures, and videos. See DOI: 10.1039/x0xx00000x

A list of materials and additional methodological details are included in electronic supporting information (ESI).

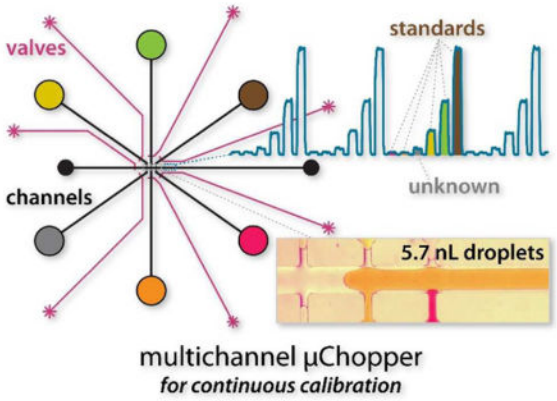

Introduction

During the past few decades of advancements in the field of microfluidics, one of the most notable analytical advantages has been the ability to sample and analyse extraordinarily small volumes of sample. As envisioned in early reports [1], integrated microsystems, i.e. micro-total analysis systems (µTAS), have since been proven capable of rapid analysis of sub-microliter samples such as whole blood, nasal aspirates, etc. [2]. Advancements in nanoliter-scale sample preparation [3–5], enzyme reactions [6–11], on-chip separations [12–20], and integrated detection systems [21–26] have unleashed a large variety of platforms capable of novel impacts in the physical, chemical, biological, and medical sciences.

More recently, droplet microfluidics has emerged as a subfield with new set of advantages to accompany the classic ones. Seminal works in this area [27–32] exhibited various novel capabilities of droplet fluidics, and further advancements have shown the propensity of droplets to permit high-throughput molecular evolution [33], digital assays [34, 35], interfacing with mass spectrometry [36–39] and electrochemistry [40], and single cell analysis at genome [41], epigenome [42], and transcriptome [43, 44] levels.

One unique feature of droplet sampling that our group has developed relates to the reduction of measurement noise in optical analytical methods [45–49]. By locking the detector into the frequency and phase of droplet formation, we devised a microfluidic analogue to an optical beam chopper (µChopper) via alternating sample and reference droplets at defined patterns [45, 49]. As with electronic lock-in amplifiers, this approach modulates the signal of interest to a higher frequency, removes low frequency noise, then demodulates the signal for recovery [50–54]. Phase-locking with droplet microfluidics was first accomplished passively, where large noise reductions allowed on-chip visible absorbance in the nanomolar range [45] or fluorescence measurements of metal ions secreted from primary cells [47]. A similar passive approach was confirmed by Marz et al. for improving Raman signals on-chip [55]. Recently, we demonstrated the usefulness of on-chip pneumatic valves [56] for further signal bandwidth reduction through enhanced precision of droplet formation [49]. This advancement reduced the droplet bandwidth to 0.04 Hz and enabled fluorescein detection limits of 310 zeptomoles, quantitative single-cell fatty acid uptake in adipocytes, and attomole detection limits with homogeneous immunoassays [49].

Here, we introduce an automated, multiplexed fluidic μChopper with six aqueous input channels and an oil channel controlled by on-chip valves. This new design shows improved flexibility that allows several analytical modes, either for continuous multi-point calibration or multiplexed analysis. One of these modes, standard addition mode, is validated for homogeneous protein quantification in human serum samples, exhibiting 100- and 75-fold volume reductions in immunoassay reagents and serum samples, respectively. This work thus combines the automation capabilities [56] with the droplet phase-locking capabilities [49] given by microfluidic valves.

Experimental Methods‡

Materials and Reagents

Precursors for polydimethylsiloxane (PDMS) devices, SylgardR 184 elastomer base and curing agent, were obtained from Dow Corning (Midland, Maryland, USA). Silicon wafers were purchased from Polishing Corporation of America (Santa Clara, CA, USA). Photoresists and developers (AZ-40-XT photoresist, AZ 300 MIF developer, SU-8 photoresist and developer) were purchased from Microchem (Westborough, MA, USA). Device interfacing components such as tubing (TGY- 020-5C; 0.02 in. ID, 0.06 in. OD, 0.02 in. wall) and blunt needles (NE-223PL-C 22G) were obtained from Small Parts (Logansport, IN, USA). Fluorescein was purchased from Alfa Aesar (Ward Hill, MA, USA). Fetal bovine serum (FBS) was purchased from VWR (West Chester, Pennsylvania, USA), and human serum samples were obtained from Bioreclamation IVT (Charleston, Maryland, USA). Aquapel was purchased from Pittsburg Glass Works (Pennsylvania, USA), and surfactant-containing carrier oil solutions were made by dissolving Pico Surf 2 surfactant (Dolomite Microfluidics, Royston, UK) in HFE-7500 oil (3M, St. Paul, MN, USA) to make 1.0% w/w solution.

Microfluidic Device Fabrication

Actively-controlled, droplet generating microfluidic devices were fabricated as previously described [49]. Briefly, devices were made of two layers of patterned PDMS following standard soft lithography guidelines [57] and pneumatic valving guidelines [56] but using an in-house built UV lithography source based on 365 nm LEDs [58]. Channel layouts were designed in Adobe Illustrator, from which masks were printed at 50 800 dpi resolution by Fineline Imaging (Colorado Spring, CO). Following exposure and baking steps to create SU-8 defined valve control channel templates or AZ-defined fluidic channel templates, silicon wafers were exposed to trimethylsilyl chloride vapour for 30 min to enhance PDMS removal. After PDMS mixing, spin-coating, and curing steps, devices were peeled from the wafer, cleaned with methanol, air dried with a stream of N^2, plasma oxidized, and bonded to a glass slide. Finally, flow channels were treated with Aquapel then rinsed with methanol to give devices capable of actively-controlled, aqueous-in-oil droplet formation. Channel cross-sections were characterized as needed by slicing an assembled PDMS device with a razor and imaging the channel cross section.

Control of Active Microfluidic Valves

On-chip pneumatic valves were used in the push-up configuration and were controlled via an in-house written application in LabVIEW (National Instruments) interfaced to a control system of off-chip solenoid valves (Lee Co.; LHDA0533115H). This approach provided on-demand droplet formation from any of the six aqueous channels in patterns defined by the mode of operation, as discussed below. Actuation of valves was accomplished with a regulated pressure source of ~20 psi, and flow was driven with a vacuum applied to the outlet channel using a hand-held, 100-mL glass syringe (SGE Analytical Science).

Multichannel μChopper Characterization and Data Analysis

For device characterization, fluorescein solutions were diluted in 20 mM HEPES buffer solution (pH = 7.5) according to each mode of operation. Stock solutions were verified through absorbance at 490 nm with a spectrophotometer (Nanodrop 1000, Thermo Scientific). Fluorescence imaging or higher sensitivity fluorescence measurements on the μChopper device were performed with either a cooled CCD camera (CoolSnap HQ2; Photometrics Scientific) or with a PMT (Hamamatsu), respectively. Both detectors were interfaced with a Nikon Ti-E inverted fluorescence microscope through a green fluorescence filter cube (excitation: 470 ± 20 nm; emission: 525 ± 25 nm). For higher sensitivity measurements, a PMT was set to a sensitivity of 10^{-3} μA V^{-1} with a 0.5 ms time constant, and amplifier offset was adjusted manually. RGB color images and videos were captured with a digital camera (Nikon J1) interfaced to a tissue culture microscope (Nikon TS100F).

The microdevice was programmable, allowing operation in several analytical modes, as discussed below. The device (multichannel μChopper) included six aqueous inlets and an oil channel inlet (Figure 1A). Using pneumatic microvalves and the LabVIEW application, droplets were generated in a programmable fashion [Negou], where each droplet was moved to the region of interest (ROI), stopped, and the fluorescence emission was collected with the PMT. This phase-locking of the droplets with the detector through customized software (Figure 1C) allowed facile separation of all six signals into different data arrays. Depending on the analytical mode, several signals could be used to generate real-time calibration curves. For characterization purposes, fast Fourier transform (FFT) analysis was also carried out in Matlab. Droplets were generated at ~0.5 Hz from each of the six reservoirs, typically resulting in a total droplet frequency of ~3.2 Hz.

Homogeneous Immunoassays in Human Serum

Concentrations of albumin in human serum samples were quantified using a mix-and-read, homogeneous fluorescence immunoassay (Human Albumin FRET-PINCER Assay Kit; Mediomics, St. Louis, MO), where higher albumin levels caused decreases in fluorescence due to target-specific probe quenching. Albumin levels in human serum samples (Bioreclamation IVT) were analysed with the standard protocols as per the manufacturer's instructions using a multimode plate reader (Beckman Coulter DTX 880), and these results were compared to those of the multichannel μChopper operating in standard addition mode on the inverted fluorescence microscope. Antibody-oligonucleotide probes were diluted 25×, and standard additions ranged from 0.03 to 4.0 μg mL^{-1}. For each serum sample, 18 μL of

sample plus reagents were made in total, yet only ~5 μL of working volume was needed in each of the 6 input reservoirs of the device.

Results and discussion

Microfluidic Device Design and Modes of Operation

The six-channel μChopper design shown in Figure 1A not only addressed several of the limitations of our previous design [49] while maintaining the benefits of valve-controlled phase-locked detection, but several novel modes of operation were also enabled. The inclusion six aqueous input channels allowed sampling, calibration, and measurement to be carried out in a fully automated fashion rather than sequential addition of various samples or standard solutions to an inlet. As shown in Figure 1B–C, the oil inlet could be programmed to separate the six aqueous inlets and position nanoliter-scale droplets at the detection point (ROI shown in Figure 1A inset). This way, the superior noise rejection of the μChopper could be exploited, and we could also avoid human error introduced while manually changing solutions in previous device iterations. A video of the multichannel μChopper device operating in continuous calibration mode is shown in SI (Video S-1).

Furthermore, since the segmentation and analysis up to six samples could be automated through LabVIEW control in a variety of ways, the new device design enabled access to multiple analytical modes not normally present in typical microfluidic fluorescence measurements. A key benefit of our design is the ability to pass any one of multiple samples or standard solutions through the same tightly focused fluorescence detection point. By matching the optical probe volume to that of one single detection channel and to the droplet dimensions, focusing optics and detector sensitivity could be fully optimized [59], which would be difficult to impossible to achieve using multiple parallel microchannels. With these combined benefits, herein the μChopper was operated using one of three analytical modes: continuous calibration mode, mixed mode, or standard addition mode. Further discussion on each mode is included below. Certainly, additional analytical modes could be envisioned, but the choice was made to validate our device with these three modes.

Continuous Calibration Mode: Real-Time, 5-Point Calibration

The gray trace in Figure 2A shows a 30 s record of raw fluorescence data from the multichannel μChopper, and a zoomed view of a 2 s window of the data is shown in Figure 2B. It is clear from these data that the automation benefits of on-chip pneumatic valving permitted precise droplet positioning and temporal control. In this instance, the third droplet in the sequence of six was labeled as the sample droplet (shaded in Figure 2B), such that every sample droplet was flanked by five calibration standards to allow full calibration about every 2 seconds. In contrast to other methods using constant referencing to a single standard [45, 47, 49, 55], this approach provides novel information to be gathered in real time. The gray traces in Figure 2E show that the slope and y-intercept of the calibration could be collected and evaluated continuously, and the quality of the linear least-square fit was maintained as the R^2 value was near unity (Figure 2D). Note that for all modes, >900 calibrations were performed over the allotted time, and R^2 histograms in Figure 2D represent counts from these individual calibrations.

An important benefit of this mode of operation is that data from calibrations and sample evaluations are simultaneously collected, eliminating the need for separate calibrations and greatly simplifying the workflow of device users. This approach also opens the possibility of studying temporal responses of systems, such as reaction kinetics [29] or the dynamics of cellular function [47]. Figure 3A–B shows an example of processed data in continuous calibration mode, where the software-encoded timing allowed facile separation of relevant fluorescence data from each droplet population and even allowed stitching of the data in the time domain for a varied representation of all traces. Finally, Figure 3C shows the time-averaged calibration curve (gray) and the unknown (light gray), confirming the operation of continuous calibration mode.

Mixed Mode: Real-Time Calibration with Multiplexed Sampling

To give one example of the multiplexing capability of the device, we show that the device can be operated in “mixed mode,” which combines a real time, three-point calibration with droplet formation from three different samples. The blue trace in Figure 2A shows a 30 s record of raw fluorescence data, and a zoomed view is again shown in Figure 2B. During one automated cycle, three samples were segmented into nanoliter droplets and positioned at the detection ROI, followed by three calibration standards. Again, the slope and y-intercept of the calibration could be evaluated continuously, and the quality of the linear least-square fit was maintained as the R^2 value was near unity (blue data in Figure 2D–E). It is obvious that the device could also be used with various combinations of samples/standards (e.g. five samples with one reference), or we could feasibly modify the device design by increasing the number of input channels to allow mixed mode with more than three samples while maintaining constant calibration. Figure 3C shows the time-averaged calibration curve (blue) and the unknown (light blue), confirming the operation of mixed mode for multiplexed analysis.

Standard Addition Mode: Matrix Corrections in Real-Time

For clinical or biochemical analyses, it is often necessary to evaluate analyte concentrations in the presence of a complex background matrix such as serum, tissue, cell lysates, soil, etc. In such cases, an effective and time-tested analytical method is the method of standard addition, where a sample aliquot is analysed alongside aliquots spiked with increasing amounts of standard solutions of the analyte of interest [53]. The magenta trace in Figure 2A shows a 30 s record of raw fluorescence data from standard addition mode, and a zoomed view is shown in Figure 2B. During an automated cycle, the sample was segmented and detected followed by five standard-spiked samples. Once again, the slope, y-intercept, and R^2 value of the calibration were continuously determined (magenta data in Figure 2D–E). Figure 3C shows the time-averaged standard addition curve (magenta points), and in this case the x-intercept is marked (light magenta) to representing the result of the standard addition analysis. This standard addition methodology was further validated by applying to quantification of proteins in human serum, as discussed in detail below.

Fourier Analysis

For all three analytical modes discussed above, we also characterized the frequency responses of the μChopper. FFT analysis was performed on raw data as in Figure 2A, which

resulted in the complex spectra shown in Figure 2C. Despite the increased complexity compared to previous μChopper characterizations [45, 49], a consistent pattern emerged as a result of the six-droplet pattern. Regardless of the analytical mode used, six dominant frequency-domain peaks were present. The first peak represented the frequency of the complete six-droplet pattern (~0.54 Hz), while the sixth peak represented the individual droplet frequency (~3.2 Hz). Harmonic patterns were also present at higher frequencies (>5 Hz), which is to be expected from the approximate square-wave signals generated by droplets passing the detection ROI. Importantly, this analysis once again confirmed the exquisite control offered by on-chip pneumatic valving; for each analytical mode tested, droplets were generated with high precision at bandwidths between 0.03 and 0.05 Hz, consistent with our recent report [49].

Testing the System with Temporal Challenges

One of the purported advantages of the multichannel μChopper is the ability to monitor dynamic changes in a sample. To exhibit this capability, we introduced a small volume spike of high concentration fluorescein into the sample reservoir (away from the microchannel entrance) while running the device in continuous calibration mode for nearly 20 min. As the diffusional mixing of fluorescein occurred, its concentration in the segmented aqueous droplets gradually increased. The leftmost data in Figure 4A shows the processed, stitched traces from each standard solution, and the corresponding quantitative data in Figure 4B shows the expected gradual increase in fluorescein concentration as the spiked standard was diffusing from the reservoir into the droplet generator. The gray calibration curve in Figure 4C shows a time-averaged curve representative of the real-time calibrations used to generate quantitative data in Figure 4B. Next, we challenged the analytical system by manually adjusting the PMT sensitivity and amplifier offset during data collection, which occurred over a time of ~1 min just after the 12 min time point. Since the PMT would respond rapidly (amplifier set to 0.5 ms time constant), this 1-minute change period was the time needed for the user to adjust both the amplification ratio and offset settings; thus the 1-minute period was essentially unimportant to the experiment at hand. The change is marked by a dashed blue line and “before” and “after” labels in the figure. The PMT sensitivity was reduced by about 20%, and the offset setting was adjusted to bring the voltage into the detection range of the analog-to-digital converter. It is clear from the data in Figure 4A that the voltage range of fluorescence emission measurements was reduced for the same calibration standards. The effects of this manual adjustment can be seen more clearly in Figure 4D where the slope abruptly decreased, the y-intercept abruptly increased, and the R^2 was reduced briefly during the adjustment starting just after the 12 min time point. The time averaged calibration curve after the change is shown by the magenta data points and line in Figure 4C.

It is clear from the quantified unknown concentration traces over time in Figure 4B that the μChopper’s continuous calibration mode was able to compensate for these abrupt and significant changes to the detector circuitry, as the trajectory of the varying fluorescein concentration was essentially unaltered. This result demonstrates one of the major benefits of the continuous, five-point calibration capability of the multichannel μChopper device. Not only can sample measurements be made on a real-time, continuous basis without the need

for separate calibrations, but the system is also capable of adjusting to environmental changes without compromising the quantitative results in longer term experiments.

Standard Addition Mode Applied to Human Serum

Lastly, we validate the device for quantification of protein in complex matrices. Specifically, homogeneous immunoassays were used to quantify albumin in human serum samples. Four different human serum samples were analysed individually using standard addition mode to correct for background fluorescence interferences, and continuous calibrations were used as depicted in Figures 2 and 3C (magenta data) to determine the x-intercept then adjust for sample dilutions. As shown in Figure 5, the μChopper results matched well with standard methodology for all four human serum samples, validating the quantitative methodology. Although higher measurement precision was expected in the μChopper results, the precision was comparable to the standard methodology, suggesting the variability to be a feature of the antibody-oligonucleotide based assay, not the measurement technique.

Along with than the rapid, automated analysis (~1.5 min) in these experiments, an important advantage provided by the μChopper was that only ~1.2 μL of total reagents and sample was needed to conduct full, six-point standard addition curves on each serum sample (0.2 μL from each of 6 reservoirs; or 35 droplets at 5.7 nL droplet volume). In fact, this represented a mere 32 pL of serum sample needed for each standard addition curve, since the serum dilution factor for these assays was 3.75×10^4. Of course, since albumin concentrations in serum were rather high, this dilution factor was necessarily high. Nonetheless, a drastic decrease in immunoassay reagents was afforded using our device, with which albumin quantification for kidney disease monitoring could be significantly simplified by coupling to very small-volume blood sampling method such as nanoneedle samplers. Compared to the plate reader based control assays, the μChopper required only 1.0% of the reagents and 1.3% of the serum sample, representing 100-fold and 75-fold reductions in cost to reach comparable analytical results (Figure 5). This improvement results from the combined effects of small volume sampling with the dramatic noise reduction provided by our phase-locked μChopper, and it should be readily extendable to other homogeneous immunoassays, mix-and-read enzyme assays, etc. For studies on limited biological samples such as single cells or small tissue sections, this approach could be enabling for multiplexed analysis or highly resolved temporal measurements.

Conclusions

An improved generation of the droplet-based μChopper was designed and validated for rapid, automated, continuous calibration of segmented (aqueous-in-oil) samples. The device's capability to accommodate up to six different aqueous solutions enabled operation in several analytical modes, namely continuous calibration, mixed, and standard addition modes. This analytical flexibility, combined with the superior permitted full calibrations to be performed at ~0.5 Hz (every ~2 s), continuous tracking of calibration quality (R^2), and real-time correction of dynamic sample- and environment-dependent changes.

Results from standard addition analyses in human serum exemplified the drastic sample and reagent volume reductions typical in microfluidic analysis systems [1, 2]. Merely 32 pL of

each serum sample and 100-fold reductions in antibody-oligonucleotide reagents were needed to conduct full, sixpoint standard addition curves with the multichannel μChopper device. While such homogeneous immunoassay reagents can be expensive at larger assay volumes, this microfluidic system enabled dramatic decreases in required reagents, giving a considerable reduction in assay cost. This device could therefore represent an enabling tool that allows prohibitively expensive assays to be considered—even highly multiplexed—in cases where standard laboratory scale analysis would be impractical. Alternatively, one or a few assays could be used to leverage high temporal resolution sampling into droplets with the new continuous calibration method. Overall, the small-volume requirements of the multichannel μChopper could prove invaluable in analysing precious specimens (cells, tissues, biological reagents) or in quantifying samples of limited volume.

Acknowledgments

The authors would like to dedicate this manuscript to Professors James P. Landers and Susan M. Lunte as a celebration of their 60th birthdays, for their pioneering and continuing work in the science of microfluidics, and for their strong contributions to education and training in the area. Also acknowledged is the generous funding for this work, provided by the National Institutes of Health, R01 DK093810.

Notes and references

1. Manz A, Graber N, Widmer HM. Sensor Actuat BChem. 1990; 1:244–248.
2. Easley CJ, Karlinsey JM, Bienvenue JM, Legendre LA, Roper MG, Feldman SH, Hughes MA, Hewlett EL, Merkel TJ, Ferrance JP, Landers JP. Proc Natl Acad Sci U S A. 2006; 103:19272–19277. [PubMed: 17159153]
3. Legendre LA, Bienvenue JM, Roper MG, Ferrance JP, Landers JP. Analytical chemistry. 2006; 78:1444–1451. [PubMed: 16503592]
4. Sonker M, Knob R, Sahore V, Woolley AT. Electrophoresis. 2017; 38:1743–1754. [PubMed: 28272749]
5. Sonker M, Sahore V, Woolley AT. Analytica Chimica Acta. 2017; 986:1–11. [PubMed: 28870312]
6. Bird CD, Emery NJ. Proc Natl Acad Sci U S A. 2009; 106:10370–10375. [PubMed: 19478068]
7. Huhmer AFR, Landers JP. Analytical chemistry. 2000; 72:5507–5512. [PubMed: 11080907]
8. Lagally ET, Medintz I, Mathies RA. Analytical chemistry. 2001; 73:565–570. [PubMed: 11217764]
9. Liu P, Mathies RA. Trends in biotechnology. 2009; 27:572–581. [PubMed: 19709772]
10. Oda RP, Strausbauch MA, Huhmer AFR, Borson N, Jurrens SR, Craighead J, Wettstein PJ, Eckloff B, Kline B, Landers JP. Analytical chemistry. 1998; 70:4361–4368. [PubMed: 9796420]
11. Schrell AM, Roper MG. Analyst. 2014; 139:2695– 2701. [PubMed: 24448431]
12. Beyor N, Yi LN, Seo TS, Mathies RA. Analytical chemistry. 2009; 81:3523–3528. [PubMed: 19341275]
13. DuVall JA, Le Roux D, Thompson BL, Birch C, Nelson DA, Li JY, Mills DL, Tsuei A, Ensenberger MG, Sprecher C, Storts DR, Root BE, Landers JP. Analytica Chimica Acta. 2017; 980:41–49. [PubMed: 28622802]
14. Easley CJ, Karlinsey JM, Landers JP. Lab on a Chip. 2006; 6:601–610. [PubMed: 16652175]
15. Saylor RA, Lunte SM. Journal of Chromatography A. 2015; 1382:48–64. [PubMed: 25637011]
16. Saylor RA, Lunte SM. Electrophoresis. 2018; 39:462–469. [PubMed: 28737835]
17. Sonker M, Parker EK, Nielsen AV, Sahore V, Woolley AT. Analyst. 2018; 143:224–231.
18. Thaitrong N, Liu P, Briese T, Lipkin WI, Chiesl TN, Higa Y, Mathies RA. Analytical chemistry. 2010; 82:10102–10109. [PubMed: 21114282]
19. Wang M, Roman GT, Perry ML, Kennedy RT. Analytical chemistry. 2009; 81:9072–9078. [PubMed: 19803495]

20. Yi L, Wang X, Dhumpa R, Schrell AM, Mukhitov N, Roper MG. Lab on a Chip. 2015; 15:823–832. [PubMed: 25474044]
21. Holcomb RE, Kraly JR, Henry CS. Analyst. 2009; 134:486–492. [PubMed: 19238284]
22. Johnson AS, Mehl BT, Martin RS. Analytical Methods. 2015; 7:884–893. [PubMed: 25663849]
23. Mehl BT, Martin RS. Analytical Methods. 2018; 10:37–45. [PubMed: 29707044]
24. Redman EA, Ramos-Payan M, Mellors JS, Ramsey JM. Analytical chemistry. 2016; 88:5324–5330. [PubMed: 27100069]
25. Santos MSF, da Costa ET, Gutz IGR, Garcia CD. Analytical chemistry. 2017; 89:1362–1368. [PubMed: 27992170]
26. Vickers JA, Dressen BM, Weston MC, Boonsong K, Chailapakul O, Cropek DM, Henry CS. Electrophoresis. 2007; 28:1123–1129. [PubMed: 17340646]
27. Huebner A, Olguin LF, Bratton D, Whyte G, Huck WTS, de Mello AJ, Edel JB, Abell C, Hollfelder F. Analytical chemistry. 2008; 80:3890–3896. [PubMed: 18399662]
28. Link DR, Anna SL, Weitz DA, Stone HA. Physical Review Letters. 2004:92.
29. Song H, Ismagilov RF. Journal of the American Chemical Society. 2003; 125:14613–14619. [PubMed: 14624612]
30. Thorsen T, Roberts RW, Arnold FH, Quake SR. Physical Review Letters. 2001; 86:4163–4166. [PubMed: 11328121]
31. Wheeler AR, Moon H, Bird CA, Loo RRO, Kim CJ, Loo JA, Garrell RL. Analytical chemistry. 2005; 77:534–540. [PubMed: 15649050]
32. Wheeler AR, Moon H, Kim CJ, Loo JA, Garrell RL. Analytical chemistry. 2004; 76:4833–4838. [PubMed: 15307795]
33. Tran DT, Cavett VJ, Dang VQ, Torres HL, Paegel BM. Proc Natl Acad Sci U S A. 2016; 113:14686– 14691. [PubMed: 27940920]
34. Eastburn DJ, Sciambi A, Abate AR. PLoS One. 2013:8.
35. Hindson BJ, Ness KD, Masquelier DA, Belgrader P, Heredia NJ, Makarewicz AJ, Bright IJ, Lucero MY, Hiddessen AL, Legler TC, Kitano TK, Hodel MR, Petersen JF, Wyatt PW, Steenblock ER, Shah PH, Bousse LJ, Troup CB, Mellen JC, Wittmann DK, Erndt NG, Cauley TH, Koehler RT, So AP, Dube S, Rose KA, Montesclaros L, Wang SL, Stumbo DP, Hodges SP, Romine S, Milanovich FP, White HE, Regan JF, Karlin-Neumann GA, Hindson CM, Saxonov S, Colston BW. Analytical chemistry. 2011; 83:8604– 8610. [PubMed: 22035192]
36. Baker CA, Roper MG. Analytical chemistry. 2012; 84:2955–2960. [PubMed: 22384846]
37. Kirby AE, Wheeler AR. Lab on a Chip. 2013; 13:2533–2540. [PubMed: 23412052]
38. Pei JA, Li QA, Kennedy RT. Journal of the American Society for Mass Spectrometry. 2010; 21:1107– 1113. [PubMed: 20219390]
39. Sun SW, Slaney TR, Kennedy RT. Analytical chemistry. 2012; 84:5794–5800. [PubMed: 22656268]
40. Lin XY, Hu XQ, Bai ZQ, He QH, Chen HW, Yan YZ, Ding ZH. Analytica Chimica Acta. 2014; 828:70–79. [PubMed: 24845817]
41. Lan F, Demaree B, Ahmed N, Abate AR. Nature biotechnology. 2017; 35:640.
42. Rotem A, Ram O, Shoresh N, Sperling RA, Goren A, Weitz DA, Bernstein BE. Nature biotechnology. 2015; 33:1165–U1191.
43. Macosko EZ, Basu A, Satija R, Nemesh J, Shekhar K, Goldman M, Tirosh I, Bialas AR, Kamitaki N, Martersteck EM, Trombetta JJ, Weitz DA, Sanes JR, Shalek AK, Regev A, McCarroll SA. Cell. 2015; 161:1202–1214. [PubMed: 26000488]
44. Zheng GXY, Terry JM, Belgrader P, Ryvkin P, Bent ZW, Wilson R, Ziraldo SB, Wheeler TD, McDermott GP, Zhu JJ, Gregory MT, Shuga J, Montesclaros L, Underwood JG, Masquelier DA, Nishimura SY, Schnall-Levin M, Wyatt PW, Hindson CM, Bharadwaj R, Wong A, Ness KD, Beppu LW, Deeg HJ, McFarland C, Loeb KR, Valente WJ, Ericson NG, Stevens EA, Radich JP, Mikkelsen TS, Hindson BJ, Bielas JH. Nature Communications. 2017:8.
45. Deal KS, Easley CJ. Analytical chemistry. 2012; 84:1510–1516. [PubMed: 22191400]
46. DeJournette CJ, Kim J, Medlen H, Li XP, Vincent LJ, Easley CJ. Analytical chemistry. 2013; 85:10556– 10564. [PubMed: 24070333]

47. Easley CJ, Rocheleau JV, Head WS, Piston DW. Analytical chemistry. 2009; 81:9086–9095. [PubMed: 19874061]
48. Godwin LA, Deal KS, Hoepfner LD, Jackson LA, Easley CJ. Analytica Chimica Acta. 2013; 758:101–107. [PubMed: 23245901]
49. Negou JT, Avila LA, Li XP, Hagos TM, Easley CJ. Analytical chemistry. 2017; 89:6154–6160.
50. Goree J. Rev Sci Instrum. 1985; 56:1662–1664.
51. Horowitz P, Hill W. The art of electronics. 2. Cambridge University Press; Cambridge England ; New York: 1989.
52. Mandelis A. Rev Sci Instrum. 1994; 65:3309–3323.
53. Skoog DA, Holler FJ, Crouch SR. Principles of instrumental analysis. 6. Thomson Brooks/Cole; Belmont, CA: 2007.
54. Wilmshurst TH. Signal recovery from noise in electronic instrumentation. 2. Hilger A, editorBristol England; Philadelphia: 1990.
55. Marz A, Bocklitz T, Popp J. Analytical chemistry. 2011; 83:8337–8340. [PubMed: 21916424]
56. Unger MA, Chou HP, Thorsen T, Scherer A, Quake SR. Science. 2000; 288:113. [PubMed: 10753110]
57. Duffy DC, McDonald JC, Schueller OJ, Whitesides GM. Analytical chemistry. 1998; 70:4974–4984. [PubMed: 21644679]
58. Erickstad M, Gutierrez E, Groisman A. Lab Chip. 2015; 15:57–61. [PubMed: 25322205]
59. Johnson ME, Landers JP. Electrophoresis. 2004; 25:3513–3527. [PubMed: 15565706]

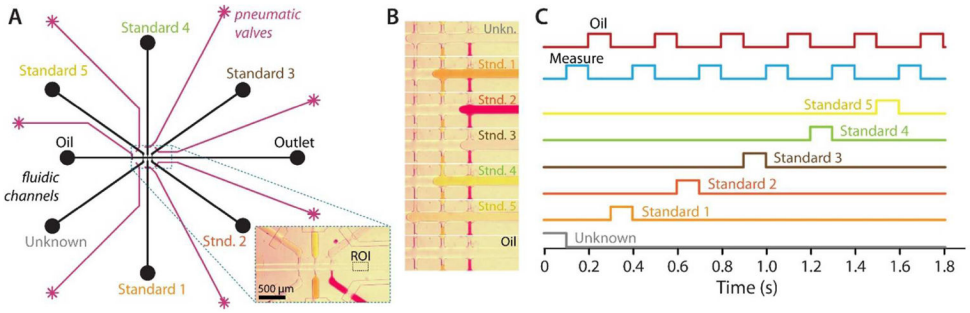

Figure 1.

Multichannel µChopper device design and operation. **(A)** The channel layout shows flow channels (black), control channels (magenta), and labels for various fluidic inlets and the waste outlet. The inset image shows the device in operation, where the region-of-interest (ROI) marking the fluorescence detection point is defined. **(B)** A montage of snapshots is shown during typical device operation in continuous calibration mode (see Video S-1 in SI), and **(C)** the temporal program for one full cycle of automated valve control is shown, where droplet positioning was phase-locked with the detector's measurement timing.

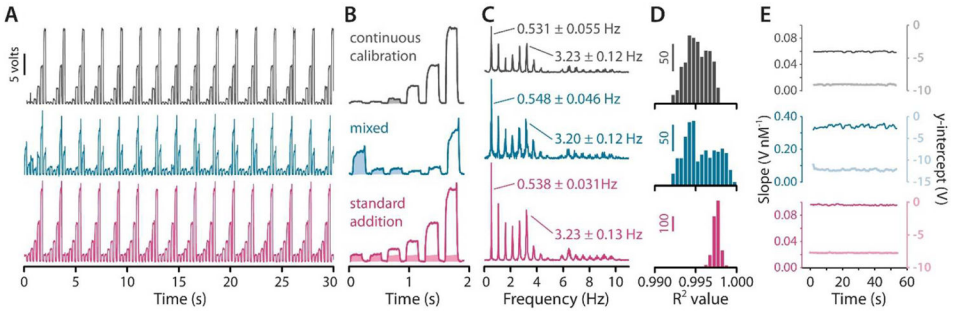

Figure 2.

Data for 3 example modes of operation using the multichannel μChopper. **(A)** Raw temporal data traces are shown for continuous calibration (gray), mixed (blue), and standard addition (magenta) modes. Scale bar denotes 5 volts for all y-axes. **(B)** Zoomed views of 2-second windows of data from (A). **(C)** Fourier analysis revealed complex spectra but confirmed high droplet generation precision. **(D)** Continuous linear least squares analysis (>900 calibrations each) exhibited consistent high quality, with R^2 values near 1.0. Scale bars denote indicated histogram counts. **(E)** Calibration metrics such as slope and y-intercept could be evaluated continuously and used for real-time quantification.

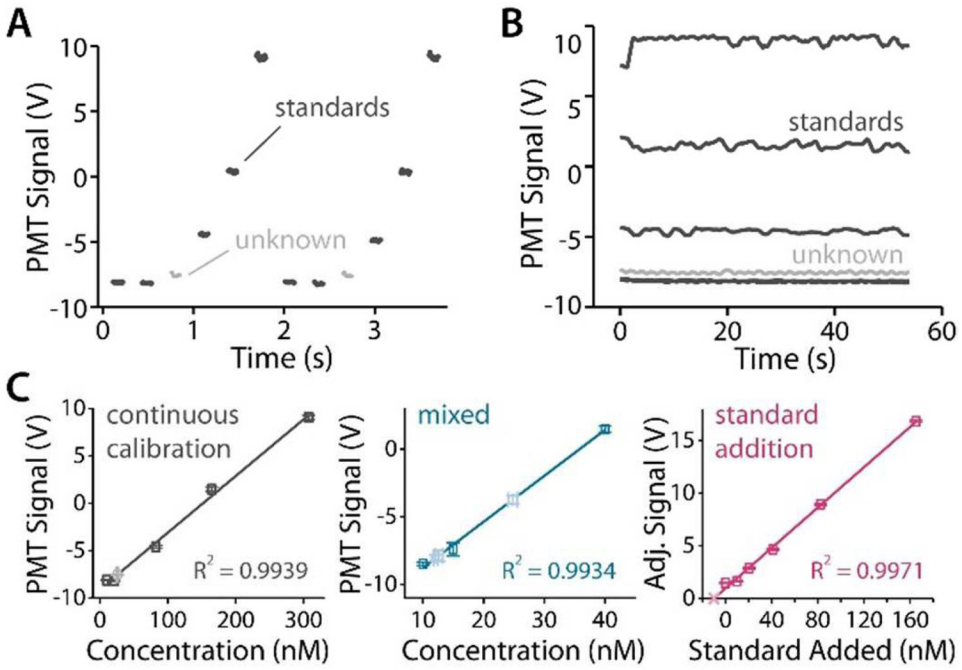

Figure 3.

Processed data. **(A)** Relevant temporal data from continuous calibration mode is shown, where software was used to automatically remove between-droplet signals. **(B)** Stitched data from each reservoir revealed consistent signals from each standard (gray) and the unknown (light gray). **(C)** Time-averaged calibration curves from each mode show the consistency provided by the μChopper. Unknown sample measurements are shown in lighter shades than the standards.

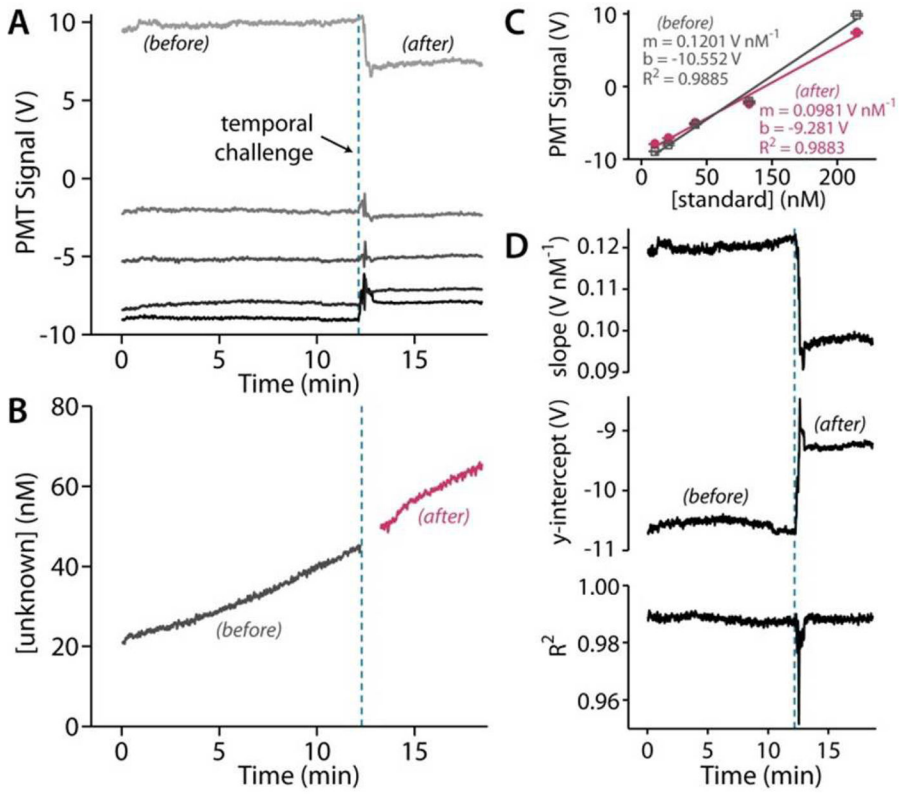

Figure 4.

The device operating in continuous calibration mode was challenged with a rapid temporal change in PMT sensitivity and offset settings (marked by dashed blue lines). Despite the drastic change in instrument settings, the multichannel μChopper was able to compensate for this change due to the real-time, five-point continuous calibration. Here, the effect is validated by **(A)** time traces of standard droplets, **(B)** the time trace of the unknown droplets, **(C)** the cumulative calibration curves before and after the challenge, and **(D)** the calibration metrics of slope, y-intercept, and R^2.

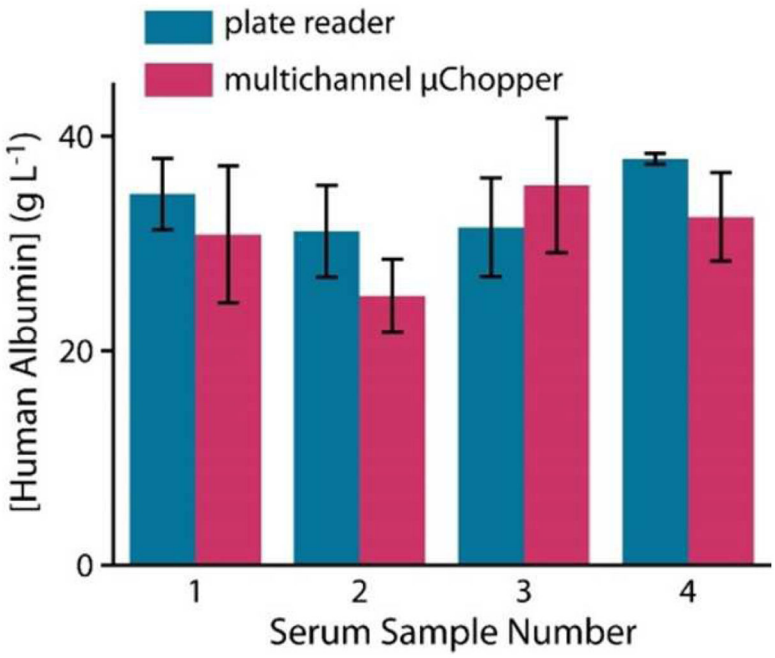

Figure 5.

Homogeneous, mix-and-read immunoassays were successfully employed within droplets for analysis of human serum samples. Using standard addition mode of the multichannel μChopper, background fluorescence from serum could be essentially negated, and full 6-point standard addition curves were carried out with 100- and 75- fold reductions in reagent and serum volumes, respectively. On-chip results (magenta) correlated well with the standard plate reader method (blue). Error bars represent standard deviations on triplicate plate reader analyses or 35-droplet analyses on-chip.